Biophysical Journal
Article

Biophysical Society

Molecular State of the Membrane-Active Antibiotic Daptomycin

Ming-Tao Lee,[1,2] Wei-Chin Hung,[3] Meng-Hsuan Hsieh,[4] Hsiung Chen,[1] Yu-Yung Chang,[1] and Huey W. Huang[5,*]
[1]National Synchrotron Radiation Research Center, Hsinchu, Taiwan; [2]Department of Physics, National Central University, Jhongli, Taiwan; [3]Department of Physics, R. O. C. Military Academy, Fengshan, Kaohsiung, Taiwan; [4]Institute of Biotechnology, National Taiwan University, Taipei, Taiwan; and [5]Department of Physics and Astronomy, Rice University, Houston, Texas

ABSTRACT Membrane-active antibiotics are potential alternatives to the resistance-prone conventional antibiotics. Daptomycin, a cyclic lipopeptide, is the only membrane-active antibiotic approved by the U.S. Food and Drug Administration so far. The drug interacts with the cytoplasmic membranes of Gram-positive pathogens, causing membrane permeabilization to ions and cell death. The antibiotic activity is calcium-ion dependent and correlates with the target membrane's content of phosphatidylglycerol (PG). For such a complex reaction with membranes, it has been difficult to uncover the molecular process that underlies its antibacterial activity. The role of the cofactor, calcium ions, has been confusing. Many have proposed that calcium ions binding to daptomycin is a precondition for membrane interaction. Here, we report our findings on the molecular state of daptomycin before and after its membrane-binding reaction, particularly at therapeutic concentrations in the low micromolar range. We were able to perform small-angle x-ray scattering at sufficiently low daptomycin concentrations to determine that the molecules are monomeric before membrane binding. By careful circular dichroism (CD) analyses of daptomycin with Ca^{2+} and PG-containing membranes, we found that there are only two states identifiable by CD, one before and another after membrane binding; all other CD spectra are linear combinations of the two. Before membrane binding, the molecular state of daptomycin as defined by CD is the same with or without calcium ions. We are able to determine the stoichiometric ratios of the membrane-binding reaction. The stoichiometric ratio of daptomycin to calcium is 2:3. The stoichiometric ratio of daptomycin to PG is ~1:1 if only the PG lipids in the outer leaflets of membranes are accessible to daptomycin.

INTRODUCTION

Daptomycin, a cyclic lipopeptide (Fig. 1), is the first U.S. Food and Drug Administration (FDA)-approved antibiotic of this new structural class (1). Clinically it is used against multidrug-resistant gram-positive pathogens, including methicillin-resistant *Staphylococcus aureus* (MRSA) and vancomycin-resistant *Enterococcus* (VRE). Accumulated evidence consistently supports the mode of action discovered 30 years ago (2–13), that its main target is the bacteria's cytoplasmic membranes, where daptomycin causes leakage of potassium ions that leads to loss of membrane potential and cell death, although there are other proposed mechanisms (e.g., (14)). The membrane function is compromised in the absence of cell lysis or leakage of molecules other than atomic ions (6,8). Many of the mutations that alter susceptibility to daptomycin have been shown to directly affect the membrane lipid composition (9–13). This further supports the role of the membrane as the primary target for the action of daptomycin. However, the molecular interaction underlying the action of daptomycin is poorly understood. Resolving the molecular mechanism is the key for understanding the cause of resistance to daptomycin during therapy (15–17). The molecular process of daptomycin-membrane interaction could reveal a so-far-unrecognized membrane-permeabilization mechanism.

It has been well established that the antibacterial activity of daptomycin is calcium-ion dependent (18) and correlates with the target membrane's content of phosphatidylglycerol (PG) (11). Indeed, daptomycin causes ion leakage from lipid vesicles only when the vesicles contain PG and only in the presence of calcium ions (19). Under this condition, fluorescence resonance energy transfer (FRET) and perylene excimer experiments detected daptomycin oligomerization (20–22). In giant unilamellar vesicles, the action of daptomycin induced visible aggregates of daptomycin and lipids to appear on the surface of membranes, hence called the lipid-extracting effect (23), although the vesicles appeared to be intact and no leakage of the small dye molecule calcein

Submitted March 30, 2017, and accepted for publication May 22, 2017.
*Correspondence: hwhuang@rice.edu
Editor: Joseph Zasadzinski.
http://dx.doi.org/10.1016/j.bpj.2017.05.025

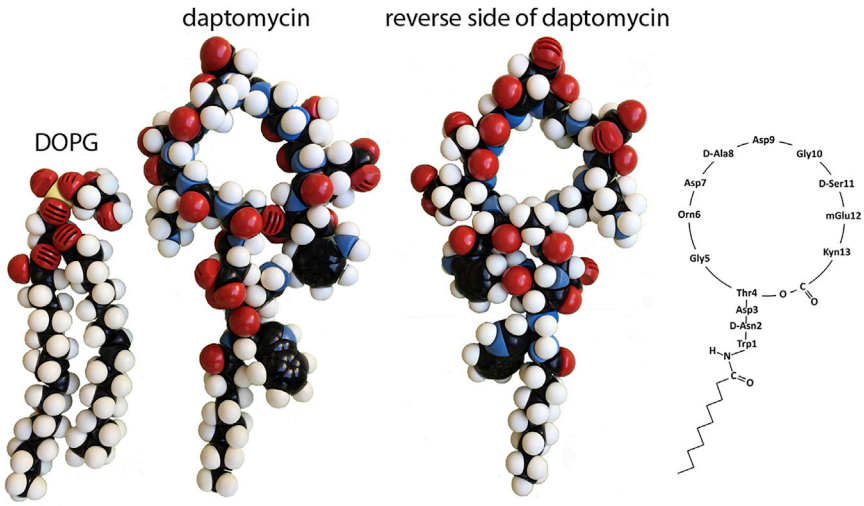

FIGURE 1 Structural formula of daptomycin with CPK space-filling atomic models. Two sides of the CPK model of daptomycin are shown along with the lipid DOPG. Their sizes are in proportion to each other. To see this figure in color, go online.

was detected from the lipid vesicles at therapeutic daptomycin concentrations (23,24).

When considering the daptomycin-membrane interactions, it is useful to compare with other membrane-active antibiotics such as the host-defense antimicrobial peptides (AMPs) (25,26). AMPs do not require cofactors for their bactericidal activities (27,28), and their actions of bacterial membrane permeabilization (29) have been reproduced in model membranes made of either charged or neutral phospholipids (30–32). In contrast, daptomycin, whose action specifically requires calcium ions in solution and PG in the membranes, is both target specific and chemically more complicated in its reaction with membranes. AMPs cause membrane permeabilization to molecules such as calcein (25,26), whereas daptomycin causes membrane permeabilization to atomic ions only (23,24). Many well-known AMPs have simple structures such as amphiphilic α-helices that provide apparent explanations for their membrane-binding affinity (e.g., melittin (33)). In contrast, daptomycin is a cyclic lipopeptide. Ten of its thirteen amino acids form a ring, and its flexibility has been detected by NMR (34–37). There are six ionizable side chains and the only apparent hydrophobic region is the decanoyl aliphatic chain acylated to the N-terminus (Fig. 1). With the possibility of complexing with Ca^{2+} ions or with both Ca^{2+} and PG headgroups, many speculative molecular complexes of daptomycin have been suggested (e.g., (38–40)).

Clearly, the molecular states of daptomycin before and after membrane binding need to be experimentally characterized to understand its action. This has been a difficult problem, partly because, unlike that of AMPs, the molecular state of daptomycin depends not only on its own concentration but also on that of Ca^{2+} ions. For instance, there were reports of daptomycin aggregation in solution (40) that led to speculation that aggregation in solution is a precondition for daptomycin's antibacterial activity (41,42). However, to understand the antibacterial activity of daptomycin, the relevant molecular state has to be that of daptomycin at its therapeutic concentrations, i.e., of the order of its minimal inhibitory concentrations, which are in the low micromolar range (4,18). The relevant Ca^{2+}-ion concentration is $\sim$1 mM, close to the concentration in human serum (4). Many of the past investigations on the molecular state of daptomycin have not been shown to cover the relevant concentrations; for example, NMR (34–37,43) and small-angle x-ray scattering (SAXS) (42) investigations were conducted in millimolar concentrations. We will also review past studies by fluorescence (41,42), isothermal calorimetry (ITC) (40), and circular dichroism (CD) (34).

Here, we report our findings at the relevant concentrations from our SAXS experiments and the CD measurements. We will show that 1) at the relevant concentrations, daptomycin is monomeric, not in aggregates; 2) there are only two molecular configurations of daptomycin, each identified by a unique ultraviolet CD spectrum, one before binding to the membranes and another after being bound to PG-containing membranes; and 3) we are able to determine the stoichiometry of the reaction among daptomycin, Ca^{2+}, and PG-containing membranes. These findings define the molecular reaction underlying daptomycin's antibacterial activity.

MATERIALS AND METHODS

Materials

Daptomycin was purchased from Selleckchem (Munich, Germany), with a high-performance liquid chromatography purity of 99.81%. 1,2-dioleoyl-*sn*-glycero-3-phosphocholine (DOPC) and 1,2-dioleoyl-*sn*-glycero-3-phospho-(1′-*rac*-glycerol) (DOPG) were purchased from Avanti Polar Lipids (Alabaster, AL). L-tryptophan, L-kynurenine, L-glycerol 3-phosphate (lithium salt), and $CaCl_2$ (purity >99%) were purchased from Sigma-Aldrich (St. Louis, MO). All purchased chemicals were used without further purification.

Unilamellar vesicles

Submicron-sized unilamellar liposomal vesicle suspensions with a low polydispersity were prepared according to published procedures (44). A

chosen lipid composition was dissolved in chloroform and dried under a gentle nitrogen flow and, subsequently, under vacuum for several hours to remove residual solvent. A 10 mM Tris buffer (pH 7.4) was added to the lipid dry film. The dispersion was shaken for 10 min and put into an ultrasonic bath for 50 min. The suspension was frozen and thawed between liquid nitrogen and 40°C water six times. To prepare for small unilamellar vesicles (SUVs), the suspension was sonified using a titanium-tip ultrasonicator for 40 min until the solution looked transparent. Titanium debris was then removed by centrifugation for 20 min at 14,000 rpm. The diameter of the vesicles was estimated by dynamic light scattering (Zetasizer Nano S90, Malvern Instruments, Malvern, United Kingdom) to be 40 $\pm$ 2 nm.

CD spectroscopy

CD spectra were measured in a Jasco (Tokyo, Japan) J-815 spectropolarimeter. For daptomycin at 4 μM, the samples were measured in a 10 mm cuvette. For daptomycin at 40 μM, the samples were measured in a 1 mm cuvette. All samples were in 10 mM Tris buffer at pH 7.4. Lipid mixtures of 7:3 DOPC/DOPG were in the form of SUVs (instead of large vesicles to avoid light scattering) and calcium ions from $CaCl_2$. Samples were thoroughly mixed before measurement. Each CD spectrum, from 280 to 200 nm, was measured in a 3 min duration, and each sample was measured twice to make sure that the spectrum did not change with time. We found that some mixtures took up to 20 min to reach equilibrium after mixing, i.e., no significant change of CD in two consecutive measurements.

SAXS

SAXS of daptomycin in 10 mM Tris buffer at pH 7.4 were measured at the BL23A SWAXS Endstation of the National Synchrotron Radiation Research Center in Hsinchu, Taiwan, with an x-ray beam of 15.0 keV (wavelength, $\lambda = 0.8267$ Å) and at a sample-to-detector distance of 1830 mm. The small-angle scattering intensities were recorded by a pixel-detector Pilatus-1MF camera (Dectris, Baden-Dättwil, Switzerland) of area 169 $\times$ 179 mm^2 and pixel resolution of 172 μm, covering the momentum transfer, Q, up to 0.5 $Å^{-1}$, which was calibrated with a standard sample of silver behenate ($Q = 4\pi \sin\theta/\lambda$, where 2θ is the angle of scattering). Each SAXS intensity profile, $I(Q)$, presented was averaged from 10 SAXS scans. The SAXS background of the solutions without daptomycin measured under the identical condition as for the sample was subtracted from the $I(Q)$. The data were normalized by the intensity of the incoming flux (45). The radius of gyration, R_g, was obtained from equating the initial slope of $\ln[I(Q)]$ to $-Q^2R_g^2/3$ (46).

RESULTS

To simulate the PG content of bacterial membranes (11), we used lipid bilayers of the DOPC/DOPG mixture at a 7:3 ratio. PC/PG mixtures have been commonly used for studies of daptomycin in model-membrane experiments, and the results are consistent with those from experiments with bacterial membranes (20,21,23,34). In the membrane-binding experiments, SUVs of the DOPC/DOPG mixture were used to diminish light scattering from vesicles, so as not to interfere with CD measurements. All samples, for both SAXS and CD experiments, were in solutions of 10 mM Tris buffer (pH 7.4) and were measured at room temperature unless specified otherwise.

SAXS of daptomycin in solution in the absence of membranes

Fig. 2 *a* shows a number of representative SAXS intensity profiles, $I(Q)$, for daptomycin at 0.5, 0.75, 1, and 2 mM with $CaCl_2$ ranging from 0 to 1 mM in 10 mM Tris buffer. More measurement results are shown in Fig. S1. The sensitivity of SAXS limited the lowest measurable daptomycin concentration to ~0.5 mM. The average radius of gyration, R_g, was obtained by equating the initial slope of $\ln[I(Q)]$ to $-Q^2R_g^2/3$ (46) and the results of all SAXS measurements are shown in Fig. 2 *b*. The SAXS intensity, $I(Q)$, curves were reversible with changes of daptomycin concentration (for example, by dilution). As the daptomycin concentration increased to $>$ 0.5 mM and Ca^{2+} concentration increased from 0 to 2 mM, the Q dependence of the SAXS intensity, $I(Q)$, showed more structural features that were made possible by larger aggregates (46), and concurrently, the average radius of gyration, R_g, also increased.

The dashed lines through the intensity curves, $I(Q)$, in Fig. 2 *a* are the model fittings described under SAXS model fittings in the Supporting Material. The most important result

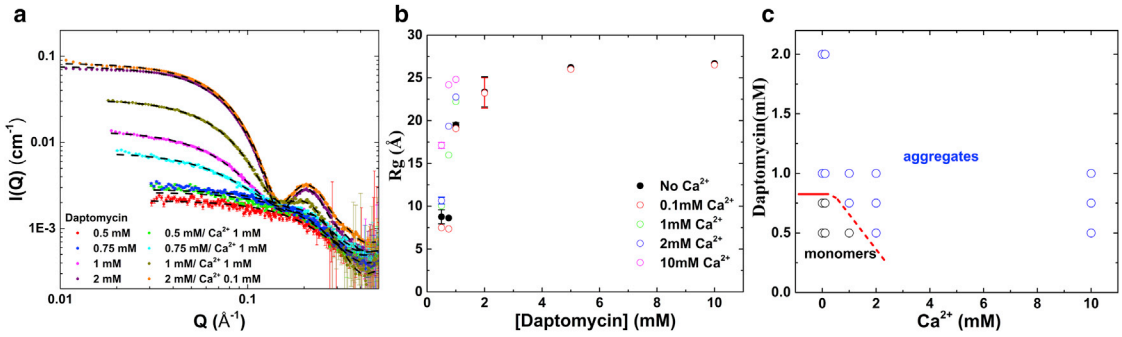

FIGURE 2 SAXS curves for daptomycin in solution. (*a*) Representative SAXS intensity profiles, $I(Q)$, at four different concentrations of daptomycin in 10 mM Tris buffer at pH 7.4 with Ca^{2+} from 0 to 1 mM. More curves are shown in Fig. S1. The black dashed lines through each individual $I(Q)$ curve are model fittings described under model fittings in the Supporting Material. (*b*) The average radius of gyration, R_g, obtained from all measured $I(Q)$ curves as a function of daptomycin concentration with Ca^{2+} from 0 to 10 mM. Multiple measurements at a given condition show the average values and standard deviations. Note that $I(Q)$ versus Q is a log-log plot—the apparent initial slope is not indicative of the R_g value. (*c*) The aggregation phase diagram for daptomycin concentration versus Ca^{2+} concentration. The red curve indicates the phase boundary, below which daptomycin is monomeric. To see this figure in color, go online.

is the fitting of a solid sphere to the $I(Q)$ of 0.5 mM daptomycin with 0 and 1 mM Ca^{2+}. The model fitting requires the radius of the sphere to be ~10.5 Å (Supporting Material) close to the theoretical value of $R_g \sim 8$ Å for a daptomycin monomer calculated by applying the CRYSOL software (47) to the structure of daptomycin obtained from the Protein Data Bank. Fig. 2 *b* shows a definitive gap between the lowest group of data with $R_g \sim 7$–10 Å and the higher data points with $R_g > \sim 16$ Å. The $I(Q)$ profiles for $R_g \sim 7$–10 Å are characteristically different from the $I(Q)$ profiles for larger R_g (Fig. 2 *a*). Thus, daptomycin at 0.5 mM concentration with Ca^{2+} concentration up to 1 mM is in the monomeric state. Fig. 2 *c* shows the monomer-versus-aggregates phase diagram of daptomycin in Ca^{2+} concentrations.

There are only two molecular states for daptomycin

Daptomycin has unique CD spectra (at least at concentrations <50 μM). In particular, there is an inversion of the sign of CD only in the presence of both calcium ions and PG lipids, as first pointed out by Jung et al. (34). We note that the equilibration time for the mixtures of daptomycin, Ca^{2+}, and PG-SUV can be as long as 20 min (see Materials and Methods). Careful measurements showed that indeed there are only two basis CD spectra for daptomycin. Figs. 3 and 4 show the CD spectra of daptomycin at 4 and 40 μM in various solution conditions. In the presence of calcium ions and PG lipids whose molar ratios to daptomycin are much higher than 1.5 and 2, respectively, there is a unique CD spectrum we will call spectrum B (Figs. 3 and 4). In any condition in which calcium ions and PG lipids are not both present, there is a unique spectrum we will call spectrum A (Figs. 3 and 4). If the condition is neither that of spectrum A nor that of spectrum B, the daptomycin CD spectrum is a linear superposition of A and B (Figs. 3 and 4). The table in Fig. 4 *e* summarizes the molecular states of daptomycin in solutions of Ca^{2+} and PG lipids. Interestingly, in the presence of L-glycerol 3-phosphate (the headgroup of PG) instead of the PG lipid, daptomycin is in the A state (Fig. 4 *b*). The B state exists only in the presence of PG-containing membranes; the PG headgroups without the hydrocarbon chains do not induce the B state. Thus, it is reasonable to assume that the A spectrum represents the solution state of daptomycin not bound to membranes. Furthermore, according to our SAXS results, the A spectrum is the spectrum for monomeric daptomycin in solution. The B state represents the state of daptomycin bound to a PG-containing membrane in the presence of Ca^{2+}. Thus the transition from A to B is the binding reaction of monomeric daptomycin to PG-containing membranes with Ca^{2+}. Since daptomycin aggregates in the presence of Ca^{2+}, and PG lipids have been detected by FRET (20–22) and observed in giant unilamellar vesicle experiments (23), daptomycin in oligomers or aggregates must be in the B state.

Selected samples have also been measured for possible temperature dependence. We found that the CD spectra of daptomycin are independent of temperature from 25 to 40°C (Fig. S2).

Stoichiometry of calcium ion and daptomycin binding to PG-containing membranes

The transition of daptomycin CD spectra from A to B was measured at 4 μM (Fig. 4 *c*) and 40 μM (Fig. 3 *b*) in the presence of excessive-PG-containing SUVs. These calcium-binding curves (in which the daptomycin and DOPC/DOPG lipid concentrations were kept at constant values) were highly reproducible, particularly at 40 μM. As expected, in a two-state equilibrium, high concentrations of substrate (unbound daptomycin) shift the equilibrium

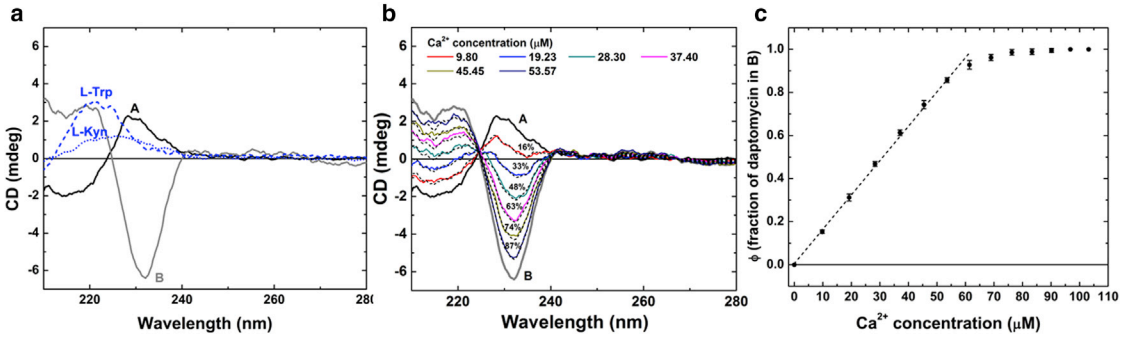

FIGURE 3 CD spectra of daptomycin and the membrane-binding stoichiometry. (*a*) Spectrum A is the CD of 40 μM daptomycin with 800 μM 7:3 DOPC/DOPG in the absence of calcium ions. Spectrum B is the CD of 40 μM daptomycin with 800 μM 7:3 DOPC/DOPG and 97 μM $CaCl_2$. The CD spectra of the single amino acids L-tryptophan and L-kynurenine in buffer solution are shown in blue. The peaks of ultraviolet absorption (data not shown) and CD of single amino acids are at the same wavelength. (*b*) CD spectra of 40 μM daptomycin with 800 μM 7:3 DOPC/DOPG in 10 mM Tris buffer at pH 7.4 at Ca^{2+} concentrations between 0 and 103 μM. Each spectrum can be fit by a linear combination of A and B spectra (*dotted lines*), with the percentage of state B indicated. (*c*) The fraction of daptomycin in the B state (ϕ) versus calcium concentration for 40 μM daptomycin with 800 μM 7:3 DOPC/DOPG, obtained from the linear fittings to the A and B spectra. The dotted line indicates daptomycin to Ca^{2+} at 2:3 mol/mol ratio. The error bars represent the range of reproducibility for three independent measurements. To see this figure in color, go online.

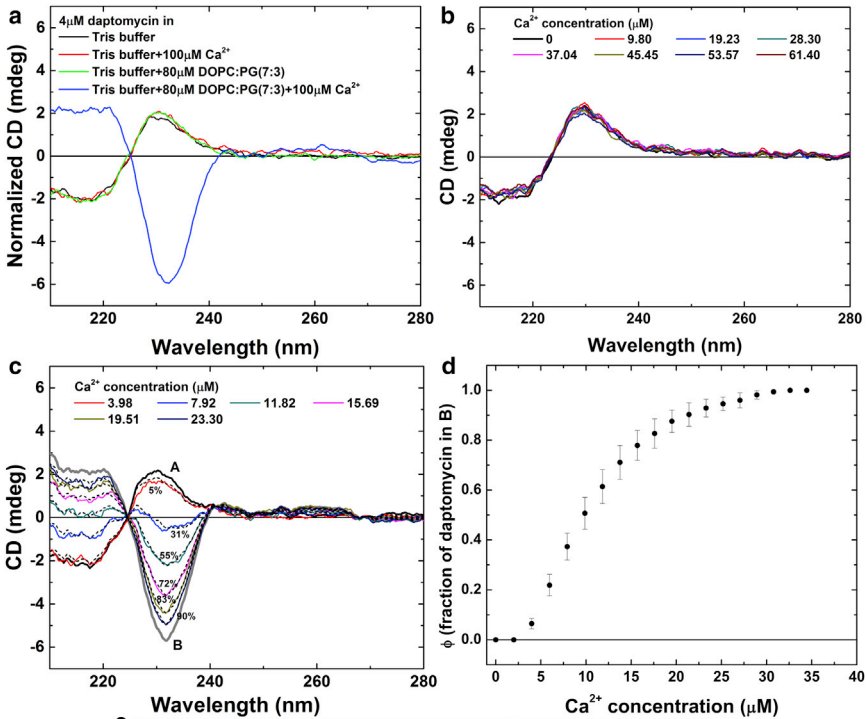

e

Molar Ratios	*CD of daptomycin (Dap)*
$Ca^{2+}/Dap = 0$ or $PG/Dap = 0$, or *both*	*A*
$Ca^{2+}/Dap \gg 3/2$ and $PG/Dap \gg 2$	*B*
$3/2 > Ca^{2+}/Dap > 0$ and $PG/Dap > 0$	*A/B mixture*
$Ca^{2+}/Dap > 0$ and $2 > PG/Dap > 0$	*A/B mixture*

FIGURE 4 More CD spectra of daptomycin. (*a*) The blue line represents the CD spectrum for 4 μM daptomycin with 80 μM 7:3 DOPC/DOPG and 100 μM $CaCl_2$, identical to spectrum B (Fig. 3 *a*). The other three lines represent the CD spectra for 4 μM daptomycin in the conditions indicated in the figure, all identical to spectrum A (Fig. 3 *a*). (*b*) CD spectra of 40 μM daptomycin, 800 μM L-glycerol 3-phosphate (the headgroup of PG) at various Ca^{2+} concentrations, all identical to spectrum A (Fig. 3 *a*). The combination of the PG headgroup and Ca^{2+} does not change daptomycin from spectrum A to spectrum B. (*c*) The CD spectra for 4 μM daptomycin with 80 μM 7:3 DOPC/DOPG at various Ca^{2+} concentrations. Each spectrum can be fit by a linear combination of A and B spectra (*dotted lines*), with the percentage of state B indicated. (*d*) Fraction of daptomycin in the B state (ϕ) versus calcium concentration for 4 μM daptomycin with 80 μM 7:3 DOPC/DOPG. The error bars represent the range of reproducibility for three independent measurements. (*e*) Summary of daptomycin CD spectra in terms of the molar ratios of Ca^{2+} to daptomycin (*Dap*) and of PG lipid to daptomycin. To see this figure in color, go online.

toward the bound state. It is apparent that daptomycin at 40 μM binds all the calcium ions in the solution up to ~60 μM, i.e., up to ~90% binding, exactly at the daptomycin/calcium ratio 2:3 (Fig. 3 *c*). Light absorption prevented CD measurement at daptomycin concentrations >40 μM, which would have shown the 2:3 stoichiometry up to 100% binding.

Next, we repeated the same calcium titration at three low lipid concentrations of 50, 100 and 200 μM (in 7:3 DOPC/DOPG) (Fig. 5). The ratio of total daptomycin to total PG was 40:15, 40:30, and 40:60, respectively. For each lipid concentration, the highest percent of A-to-B conversion is limited by the amount of PG, ~18, ~35, and ~70%, respectively. Thus, the ratio of bound daptomycin to PG is ~7:15, ~14: 30, and ~28: 60, respectively. The maximal fraction of daptomycin bound to membranes is proportional to the amount of available PG.

DISCUSSION

Molecular state of daptomycin in the absence of membranes

Aggregations of daptomycin in solution have been reported by NMR (34), sedimentation (38), fluorescence (41), dynamic light scattering (41), cryogenic-transmission electron (42), and SAXS (42). These reports have led to speculation that aggregation in solution is a precondition for daptomycin's antibacterial activity (38,41,42). However, with the exception of fluorescence measurements, all of these previous investigations were performed in the millimolar range of daptomycin concentrations. For example, NMR was typically performed at concentrations >1 mM (34–37). The results from three independent NMR investigations (34,36,37) did not agree with each other, and it was suspected that the disagreement was due to aggregations (37). SAXS and cryogenic-transmission electron microscopy (42) clearly showed daptomycin aggregations at 3 mM and higher concentrations.

The fluorescence spectrum of daptomycin has a peak at ~460 nm. The fluorescence method used by Qiu and Kirsch (41) and by Kirkham et al. (42) relied on a plot of the 460 nm fluorescence intensity as a function of daptomycin concentration. At pH values ≤4, the plot has a discontinuous increase of the slope at ~0.12 mM daptomycin, which was identified as the critical aggregation concentration. The discontinuity became unclear or absent at pH values higher >5.5, which was taken as an indication of no aggregation (41). Although this conclusion of no aggregation at pH ~7 is in agreement with the SAXS result reported

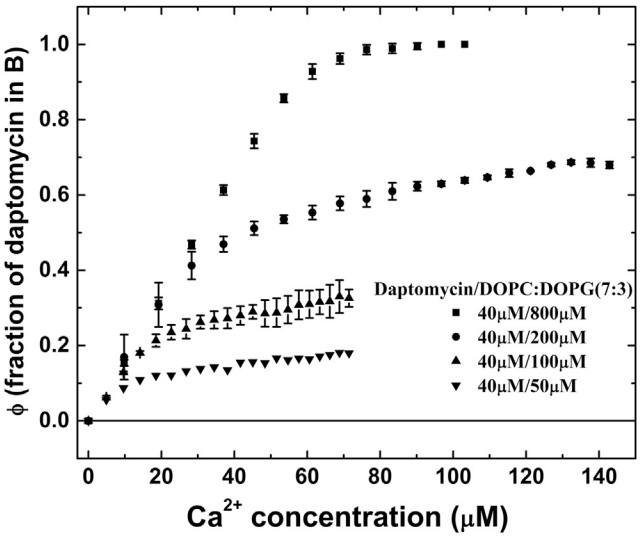

FIGURE 5 Stoichiometry of daptomycin and calcium binding to PG-containing membranes. The experimental data are the fraction of 40 μM daptomycin in the B state, ϕ, as a function of Ca^{2+} concentration at different lipid concentrations. The lipids were DOPC/DOPG 7:3 in SUVs. The error bars represent the range of reproducibility for three independent measurements.

here, we believe that the interpretation of fluorescence intensity for aggregation requires justification.

In comparison, SAXS has a simple physical basis depending only on the size of the object (46). Indeed daptomycin aggregates have been previously detected by SAXS in concentrations >3 mM; 3 mM is the lowest daptomycin concentration measured to date (42). This measurement was performed at Diamond Light Source (DLS) (Harwell, United Kingdom). Our current SAXS experiment was performed at the National Synchrotron Radiation Research Center, whose facility is similar to DLS. To measure SAXS at lower daptomycin concentrations, we used the previous measurement as a reference (see Supporting Material, SAXS comparison). To increase the signal/noise ratios, we used a shorter x-ray wavelength to reduce x-ray absorption by air and substrate, and a shorter sample-to-detector distance to reduce air absorption. We also used a sample holder with a thinner wall to reduce the absorption by the x-ray window. A table is given in the Supporting Material for comparison of the experimental parameters between the DLS measurement and ours.

We reproduced the results of the previous measurement at concentrations >3 mM. At 0.75 mM, daptomycin is monomeric at Ca^{2+} concentrations <0.1 mM, but it forms aggregates at higher Ca^{2+} concentrations. Clearly, Ca^{2+} ions have an aggregation effect. Most importantly, we were able to measure SAXS of daptomycin at 0.5 mM concentration with 1 mM Ca^{2+} at pH 7.4 (Fig. 2). Under this condition, daptomycin is unambiguously monomeric (Fig. 2, and see Supporting Material, SAXS model fittings). Thus, it is reasonable to extrapolate the result to the micromolar range and conclude that at concentrations within its minimal inhibitory concentration range, at physiological calcium concentrations of ~1 mM and pH 7.4, the solution state of daptomycin before membrane binding is monomeric.

Stoichiometry of daptomycin's membrane-binding reaction

A recent attempt to determine the daptomycin binding stoichiometry was made using ITC (39). ITC is ideal for a two-body binding isotherm, especially for non-charged binding between peptide and membrane, because in this case the reaction heat per peptide is constant (48). For charged binding, the reaction heat would change with the degree of binding; therefore, the binding isotherm of charged peptide to membrane is model dependent (48). Daptomycin binding is more complicated; it is a three-body binding involving daptomycin, Ca^{2+}, and PG-containing membranes. With a single titration of $CaCl_2$ into a solution of DOPC/DOPG vesicles (3.55–4.55 mM) and daptomycin (150–510 mM), as performed by Taylor et al. (39), the heat of reaction has no simple interpretation; therefore, the results are highly model dependent. The authors' model proposed that calcium ions bind to two sequential sites of daptomycin (39).

In comparison, our results showed that for a system of Ca^{2+}/daptomycin/PG-containing bilayers, there are only two basis CD spectra representing two distinct states of daptomycin, one for daptomycin not bound to PG-containing membranes and another for daptomycin bound to PG-containing membranes in the presence of calcium ions. In an earlier CD study (34), the CD spectrum of daptomycin in solution was shown to change by adding $CaCl_2$ or by adding PC/PG liposomes (Fig. 1 *B* in (34)). This result led to the speculation that daptomycin sequentially binds two calcium ions (34,39,40). We have re-measured these spectra and found that adding Ca^{2+} alone or adding PC/PG vesicles alone does not change the CD spectrum of daptomycin from spectrum A (Fig. 4 *a*). A possible reason for these discrepancies could have to do with whether the samples had sufficient time to reach equilibrium (see Materials and Methods). We have measured many different combinations of daptomycin, Ca^{2+}, and PG lipid (Figs. 3, 4, and 5), and found that there is no intermediate molecular state between A and B. In a two-state equilibrium between state A and state B, it is straightforward to obtain the daptomycin/calcium stoichiometry at high ligand concentrations (Fig. 3 *c*). The stoichiometric ratio of daptomycin to calcium is 2:3.

Our results also suggest a definitive stoichiometric ratio to PG, because the maximal A-to-B conversion is proportional to the PG content. Fig. 5 shows that when the PG content increased two times and four times (from 15 to 30 μM and then to 60 μM), the maximal A-to-B conversion also increased two times and four times, respectively (from ~18 to ~35% and then ~70%, respectively). The reason that the three low titration curves in Fig. 5 did not reach a clear saturation level is that it takes a long time to exhaust all available PGs

distributed among a large number of small vesicles (despite our mix-and-wait procedure; see Materials and Methods for CD). (In contrast, the top titration curve reaches a clear saturation level, because there were excessive PGs.) As a result, the approximate values for the bound daptomycin/total PG ratios of ~7:15, ~14:30, and ~28:60 from the three low titration curves slightly underestimate the possible maximal bound daptomycin. If only one-half of the total PGs, i.e., only those on the outer leaflets of vesicles, are accessible to daptomycin binding, the stoichiometric ratios of bound daptomycin to accessible PG are ~7:7.5, ~14:15, and ~28:30. Considering the possibility that the bound daptomycin is slightly underestimated, the ratios are very close to 1:1.

The CD of daptomycin and the stoichiometry of the daptomycin/Ca^{2+}/PG membrane-binding reaction are independent of temperature from 25°C to 40°C. If the spectra or the stoichiometry were sensitive to temperature, the CD spectra of state A/state B mixtures would have changed with temperature, but they do not (Fig. S2).

CD spectra of daptomycin

Daptomycin has unique CD spectra. In particular, there is an inversion of the sign of CD only in the presence of both calcium ions and PG lipids, as first pointed out by Jung et al. (34). Such CD spectra have been identified as exciton couplets of aromatic residues (49–53). The key features of both A and B spectra, from 210 to 240 nm, are that the spectra are wave-like with a sign-changing crossover near the wavelength 225 nm (Fig. 3 *a*). Daptomycin has two aromatic amino acids: tryptophan-1 and kynurenine-13 (Fig. 1). Each Trp and Kyn has a side-chain chromophore with an absorption peak near 225 nm (Fig. 3 *a*). If two chromophores are sufficiently close, their interaction can give rise to an exciton effect (49,50,53,54). The CD of daptomycin, both state A and state B, suggest an exciton coupling between two chromophores that gives rise to a splitting of the excited state into two components, one of which arises from an in-phase combination of the two monomeric excitations and the other from the out-of-phase combination (49,50,53). Hence, the rotational strengths for the two coupled states are opposite in sign, one shifted to the long-wavelength side and another shifted to the short-wavelength side, and they combine to an exciton couplet, i.e., a wave-like spectrum with a sign-changing crossover at the monomer's peak position. An exciton couplet with a positive long-wavelength band, like spectrum A, is called a positive couplet. An exciton couplet with a negative long-wavelength band, like spectrum B, is called a negative couplet (53).

The amplitude of an exciton couplet is determined by the strength of the coupling interaction, and the sign is determined by the chirality of the geometry between the two interacting transition dipoles of chromophores (49,50,53). From the SAXS experiments, we have determined that in the low micromolar range of concentration, daptomycin is monomeric. This implies that the exciton couplet spectrum A is the result of the intramolecular coupling of Trp-1 and Kyn-13.

On the other hand, we have found that the stoichiometric ratio of daptomycin to Ca^{2+} is 2:3 in their binding reaction to PG-containing membranes. The minimal number of daptomycin molecules involved in this binding reaction with an integral number of calcium ions is 2. Also, this binding reaction causes a flip of sign from positive couplet A to negative couplet B that requires a change of chirality of the geometry between two interacting chromophores (49,50,53). Thus, this reaction changes daptomycin from monomeric to dimeric (or larger, even-number multimeric) complexes with Ca^{2+} and PG. The change from monomers to dimers or multimers can include a change of couplet sign, perhaps a change from intramolecular coupling to intermolecular coupling. The dimeric (or higher multimeric) binding to membrane can also explain the detection of FRET when daptomycin binds to membranes (20–22) and the observation of daptomycin-lipid aggregates in the aforementioned lipid-extraction effect (23).

CONCLUSIONS

The complex system of daptomycin with calcium ions and PG-containing membranes has led to many speculations about the molecular state of daptomycin both before and after membrane binding. The role of various spectroscopic experiments (reviewed recently (40)) is to narrow down or provide constraints for the possible molecular-state transitions consistent with the daptomycin mechanism. The strongest constraints so far are that 1) daptomycin induces membrane permeability to atomic ions (2–13), but not to molecules such as calcein (23,24), and 2) there are indications of oligomerization (20,21) or aggregation (23) of daptomycin after binding to PG-containing membranes. Here, our results provide further constraints as follows. 1) Daptomycin before membrane binding is monomeric in its therapeutic concentrations and the monomeric daptomycin has a unique CD state independent of calcium ion concentrations. 2) Daptomycin and Ca^{2+} bind to PG-containing membranes with a stoichiometric daptomycin/calcium ratio of 2:3, and a daptomycin/PG ratio close to 1:1. This 1:1 ratio assumes that only the PGs in the outer leaflets of lipid vesicles are accessible to daptomycin. The daptomycin/PG stoichiometric ratio would be 1:2 if all the PGs in lipid vesicles were accessible to daptomycin. 3) Daptomycin has another unique CD state after its binding to PG-containing membranes with calcium ions, perhaps in oligomers (20–22) or in aggregates bound with lipids (23). The molecular processes underlying daptomycin's antibiotic activity must satisfy all of these constraints.

SUPPORTING MATERIAL

Supporting Materials and Methods and two figures are available at http://www.biophysj.org/biophysj/supplemental/S0006-3495(17)30564-7.

AUTHOR CONTRIBUTIONS

M.-T.L. and H.W.H. designed the research. M.-T.L., W.-C.H., M.-H.H., H.C., and Y.-Y.C., performed the experiments. M.-T.L. and H.W.H. analyzed the data. H.W.H. wrote the article.

ACKNOWLEDGMENTS

H.W.H. thanks Bob Woody for discussions on circular dichroism.

This work was supported by Taiwan Ministry of Science and Technology (MOST) grants 104-2112-M-213-001 (to M.-T.L.) and 104-2112-M-145-002 (to W.-C.H.), National Institutes of Health grant GM55203, and Robert A. Welch Foundation grant C-0991 (to H.W.H).

REFERENCES

1. Baltz, R. H. 2007. Antimicrobials from actinomycetes. *Microbe.* 2:125–131.
2. Allen, N. E., J. N. Hobbs, and W. E. Alborn, Jr. 1987. Inhibition of peptidoglycan biosynthesis in gram-positive bacteria by LY146032. *Antimicrob. Agents Chemother.* 31:1093–1099.
3. Silverman, J. A., N. G. Perlmutter, and H. M. Shapiro. 2003. Correlation of daptomycin bactericidal activity and membrane depolarization in *Staphylococcus aureus*. *Antimicrob. Agents Chemother.* 47:2538–2544.
4. Cottagnoud, P. 2008. Daptomycin: a new treatment for insidious infections due to gram-positive pathogens. *Swiss Med. Wkly.* 138:93–99.
5. Mascio, C. T., J. D. Alder, and J. A. Silverman. 2007. Bactericidal action of daptomycin against stationary-phase and nondividing *Staphylococcus aureus* cells. *Antimicrob. Agents Chemother.* 51:4255–4260.
6. Hobbs, J. K., K. Miller, …, I. Chopra. 2008. Consequences of daptomycin-mediated membrane damage in *Staphylococcus aureus*. *J. Antimicrob. Chemother.* 62:1003–1008.
7. Pogliano, J., N. Pogliano, and J. A. Silverman. 2012. Daptomycin-mediated reorganization of membrane architecture causes mislocalization of essential cell division proteins. *J. Bacteriol.* 194:4494–4504.
8. Cotroneo, N., R. Harris, …, J. A. Silverman. 2008. Daptomycin exerts bactericidal activity without lysis of *Staphylococcus aureus*. *Antimicrob. Agents Chemother.* 52:2223–2225.
9. Arias, C. A., D. Panesso, …, G. M. Weinstock. 2011. Genetic basis for in vivo daptomycin resistance in enterococci. *N. Engl. J. Med.* 365:892–900.
10. Friedman, L., J. D. Alder, and J. A. Silverman. 2006. Genetic changes that correlate with reduced susceptibility to daptomycin in *Staphylococcus aureus*. *Antimicrob. Agents Chemother.* 50:2137–2145.
11. Hachmann, A. B., E. Sevim, …, J. D. Helmann. 2011. Reduction in membrane phosphatidylglycerol content leads to daptomycin resistance in *Bacillus subtilis*. *Antimicrob. Agents Chemother.* 55:4326–4337.
12. Palmer, K. L., A. Daniel, …, M. S. Gilmore. 2011. Genetic basis for daptomycin resistance in enterococci. *Antimicrob. Agents Chemother.* 55:3345–3356.
13. Davlieva, M., W. Zhang, …, Y. Shamoo. 2013. Biochemical characterization of cardiolipin synthase mutations associated with daptomycin resistance in enterococci. *Antimicrob. Agents Chemother.* 57:289–296.
14. Müller, A., M. Wenzel, …, L. W. Hamoen. 2016. Daptomycin inhibits cell envelope synthesis by interfering with fluid membrane microdomains. *Proc. Natl. Acad. Sci. USA.* 201611173.
15. Munoz-Price, L. S., K. Lolans, and J. P. Quinn. 2005. Emergence of resistance to daptomycin during treatment of vancomycin-resistant *Enterococcus faecalis* infection. *Clin. Infect. Dis.* 41:565–566.
16. Lewis, J. S., 2nd, A. Owens, …, J. H. Jorgensen. 2005. Emergence of daptomycin resistance in *Enterococcus faecium* during daptomycin therapy. *Antimicrob. Agents Chemother.* 49:1664–1665.
17. Green, M. R., C. Anasetti, …, J. N. Greene. 2006. Development of daptomycin resistance in a bone marrow transplant patient with vancomycin-resistant *Enterococcus durans*. *J. Oncol. Pharm. Pract.* 12:179–181.
18. Barry, A. L., P. C. Fuchs, and S. D. Brown. 2001. In vitro activities of daptomycin against 2,789 clinical isolates from 11 North American medical centers. *Antimicrob. Agents Chemother.* 45:1919–1922.
19. Zhang, T., J. K. Muraih, …, M. Palmer. 2014. Daptomycin forms cation- and size-selective pores in model membranes. *Biochim. Biophys. Acta.* 1838:2425–2430.
20. Muraih, J. K., A. Pearson, …, M. Palmer. 2011. Oligomerization of daptomycin on membranes. *Biochim. Biophys. Acta.* 1808:1154–1160.
21. Muraih, J. K., J. Harris, …, M. Palmer. 2012. Characterization of daptomycin oligomerization with perylene excimer fluorescence: stoichiometric binding of phosphatidylglycerol triggers oligomer formation. *Biochim. Biophys. Acta.* 1818:673–678.
22. Muraih, J. K., and M. Palmer. 2012. Estimation of the subunit stoichiometry of the membrane-associated daptomycin oligomer by FRET. *Biochim. Biophys. Acta.* 1818:1642–1647.
23. Chen, Y. F., T. L. Sun, …, H. W. Huang. 2014. Interaction of daptomycin with lipid bilayers: a lipid extracting effect. *Biochemistry.* 53:5384–5392.
24. Rubinchik, E., T. Schneider, …, R. E. Hancock. 2011. Mechanism of action and limited cross-resistance of new lipopeptide MX-2401. *Antimicrob. Agents Chemother.* 55:2743–2754.
25. Boman, H. G., J. Marsh, and J. A. Goode. 1994. Antimicrobial Peptides. John Wiley and Sons, Chichester.
26. Zasloff, M. 2002. Antimicrobial peptides of multicellular organisms. *Nature.* 415:389–395.
27. Sochacki, K. A., K. J. Barns, …, J. C. Weisshaar. 2011. Real-time attack on single *Escherichia coli* cells by the human antimicrobial peptide LL-37. *Proc. Natl. Acad. Sci. USA.* 108:E77–E81.
28. Sun, Y., T. L. Sun, and H. W. Huang. 2016. Mode of action of antimicrobial peptides on *E. coli* spheroplasts. *Biophys. J.* 111:132–139.
29. Faust, J. E., P. Y. Yang, and H. W. Huang. 2017. Action of antimicrobial peptides on bacterial and lipid membranes: a direct comparison. *Biophys. J.* 112:1663–1672.
30. Matsuzaki, K. 1998. Magainins as paradigm for the mode of action of pore forming polypeptides. *Biochim. Biophys. Acta.* 1376:391–400.
31. Shai, Y. 1999. Mechanism of the binding, insertion and destabilization of phospholipid bilayer membranes by α-helical antimicrobial and cell non-selective membrane-lytic peptides. *Biochim. Biophys. Acta.* 1462:55–70.
32. Allende, D., S. A. Simon, and T. J. McIntosh. 2005. Melittin-induced bilayer leakage depends on lipid material properties: evidence for toroidal pores. *Biophys. J.* 88:1828–1837.
33. Terwilliger, T. C., L. Weissman, and D. Eisenberg. 1982. The structure of melittin in the form I crystals and its implication for melittin's lytic and surface activities. *Biophys. J.* 37:353–361.
34. Jung, D., A. Rozek, …, R. E. Hancock. 2004. Structural transitions as determinants of the action of the calcium-dependent antibiotic daptomycin. *Chem. Biol.* 11:949–957.
35. Ho, S. W., D. Jung, …, S. K. Straus. 2008. Effect of divalent cations on the structure of the antibiotic daptomycin. *Eur. Biophys. J.* 37:421–433.
36. Ball, L. J., C. M. Goult, …, V. Ramesh. 2004. NMR structure determination and calcium binding effects of lipopeptide antibiotic daptomycin. *Org. Biomol. Chem.* 2:1872–1878.
37. Rotondi, K. S., and L. M. Gierasch. 2005. A well-defined amphipathic conformation for the calcium-free cyclic lipopeptide antibiotic, daptomycin, in aqueous solution. *Biopolymers.* 80:374–385.
38. Straus, S. K., and R. E. Hancock. 2006. Mode of action of the new antibiotic for Gram-positive pathogens daptomycin: comparison with cationic antimicrobial peptides and lipopeptides. *Biochim. Biophys. Acta.* 1758:1215–1223.

39. Taylor, R., K. Butt, …, M. Palmer. 2016. Two successive calcium-dependent transitions mediate membrane binding and oligomerization of daptomycin and the related antibiotic A54145. *Biochim. Biophys. Acta.* 1858:1999–2005.

40. Taylor, S. D., and M. Palmer. 2016. The action mechanism of daptomycin. *Bioorg. Med. Chem.* 24:6253–6268.

41. Qiu, J., and L. E. Kirsch. 2014. Evaluation of lipopeptide (daptomycin) aggregation using fluorescence, light scattering, and nuclear magnetic resonance spectroscopy. *J. Pharm. Sci.* 103:853–861.

42. Kirkham, S., V. Castelletto, …, J. Ruokolainen. 2016. Self-assembly of the cyclic lipopeptide daptomycin: spherical micelle formation does not depend on the presence of calcium chloride. *ChemPhysChem.* 17:2118–2122.

43. Scott, W. R., S. B. Baek, …, S. K. Straus. 2007. NMR structural studies of the antibiotic lipopeptide daptomycin in DHPC micelles. *Biochim. Biophys. Acta.* 1768:3116–3126.

44. Rex, S. 1996. Pore formation induced by the peptide melittin in different lipid vesicle membranes. *Biophys. Chem.* 58:75–85.

45. U-Ser, J., S. H. Chiu, …, C. H. Chang. 2010. A small/wide-angle x-ray scattering instrument for structural characterization of air-liquid interfaces, thin films, and bulk speciments. *J. Appl. Crystallogr.* 43: 110–121.

46. Guinier, A. 1963. X-ray Diffraction: In Crystals, Imperfect Crystals, and Amorphous Bodies. W. H. Freeman, San Francisco, pp. 319–350.

47. Svergun, D., C. Barberato, and M. H. J. Koch. 1995. CRYSOL-a program to evaluate X-ray solution scattering of biological macromolecules from atomic coordinates. *J. Appl. Crystallogr.* 28:768–773.

48. Seelig, J. 1997. Titration calorimetry of lipid-peptide interactions. *Biochim. Biophys. Acta.* 1331:103–116.

49. Tinoco, I. 1963. The exciton contribution to the optical rotation of polymers. *Radiat. Res.* 20:133.

50. Harada, N., and K. Nakanishi. 1972. The exciton chirality method and its application to configurational and conformational studies of natural products. *Acc. Chem. Res.* 5:257–263.

51. Kuwajima, K., E. P. Garvey, …, S. Sugai. 1991. Transient intermediates in the folding of dihydrofolate reductase as detected by far-ultraviolet circular dichroism spectroscopy. *Biochemistry.* 30:7693–7703.

52. Arnold, G. E., L. A. Day, and A. K. Dunker. 1992. Tryptophan contributions to the unusual circular dichroism of fd bacteriophage. *Biochemistry.* 31:7948–7956.

53. Woody, R. W. 1994. Contributions of tryptophan side chains to the far-ultraviolet circular dichroism of proteins. *Eur. Biophys. J.* 23: 253–262.

54. Harada, N., and K. Nakanishi. 1983. Circular Dichroic Spectroscopy: Exciton Coupling in Organic Stereochemistry. University Science Books, Mill Valley, CA.

Biophysical Journal, Volume *113*

Supplemental Information

Molecular State of the Membrane-Active Antibiotic Daptomycin

Ming-Tao Lee, Wei-Chin Hung, Meng-Hsuan Hsieh, Hsiung Chen, Yu-Yung Chang, and Huey W. Huang

Supplemental Information
for **Molecular state of the membrane-active antibiotic daptomycin**

Ming-Tao Lee, Wei-Chin Hung, Meng-Hsuan Hsieh, Hsiung Chen,
Yu-Yung Chang and Huey W. Huang

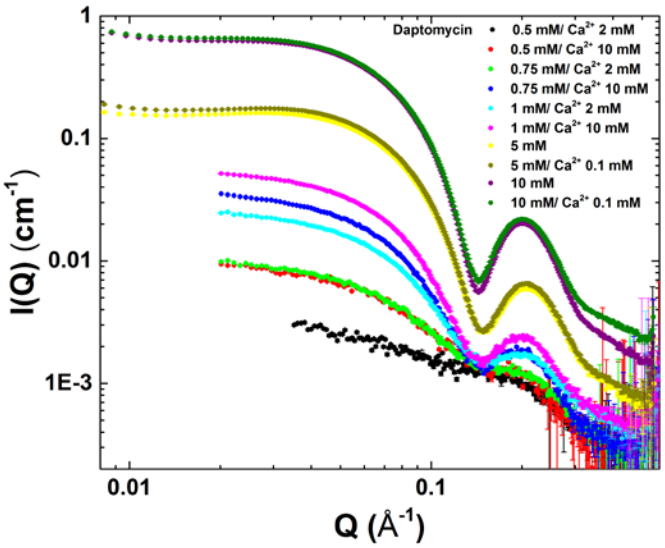

Fig. S1 More small-angle X-ray scattering curves of daptomycin in solution, supplemental to Fig. 2a. The SAXS intensity profiles *I(Q)* at five different concentrations of daptomycin in 10 mM Tris buffer at pH 7.4 with Ca^{2+} from 0.1 to 10 mM.

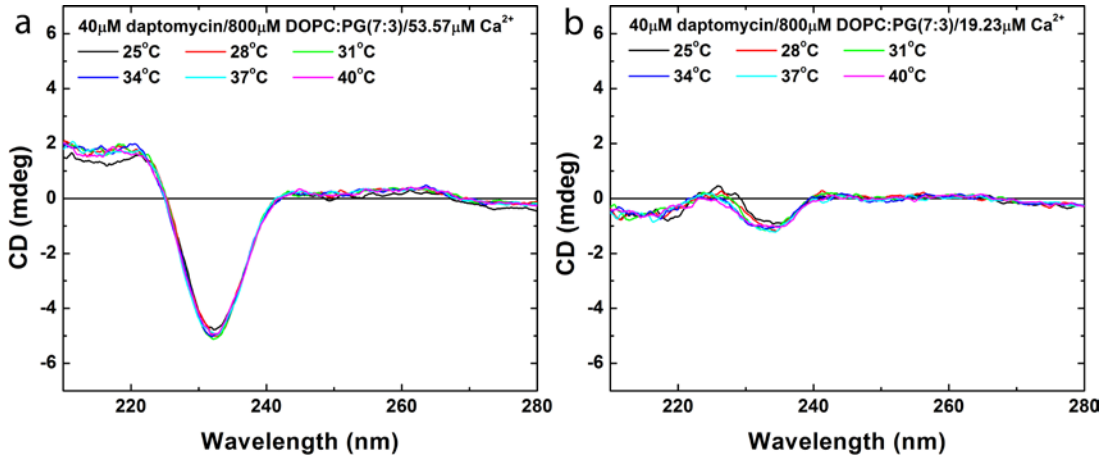

Fig. S2 Temperature dependence of daptomycin CD spectra. (a) The sample is in 13% A and 87% B mixture, shown in Fig. 3b. (b) The sample is in 67% A and 33% B mixture, shown in Fig. 3b. We allowed 20 min for sample to reach equilibrium at each temperature. There is no detectable temperature dependence from 25° C to 40° C.

SAXS comparison

Our SAXS measurement at NSSRC vs. Kirkham et al. (2016) at Diamond Light Source (DLS)

	NSRRC (BL23A beamline)	DLS (B21 beamline)
Flux (photons/s)	10^{11}	10^{11}
Photon energy (keV)	15	12.4
Detector	Pilatus 1M	Pilatus 2M
Sample to detector distance	1.83 m	4.01 m
Sample cell	Quartz cuvette with 30 μm window	Capillary with 100 μm wall

SAXS model fittings

The SAXS data were modeled by using the software SasView (http://www.sasview.org/ originally developed by the DANSE project under NSF award DMR-0520547). Solid sphere, core shell and RaspBerry models were used in the low, medium and high daptomycin concentrations respectively. The main parameters are listed in the following table: the fittings are shown in Fig. 1a.

(a) Sphere model

Daptomycin (mM)	Ca^{2+} (mM)	R (Å)
0.5	0	10.35
0.5	1	10.60
0.75	0	10.28

(b) Core shell model

Daptomycin (mM)	Ca^{2+} (mM)	R_{in} (Å)	R_{out} (Å)
0.75	1	9.98	39.59
1	0	10.41	37.86

(c) RaspBerry model

Daptomycin (mM)	Ca^{2+} (mM)	R_o (Å)	R_p (Å)	b (Å)	N
1	1	19.27	10.67	9.07	28
2	0	20.47	10.26	6.77	28
2	1	19.96	10.15	7.00	28

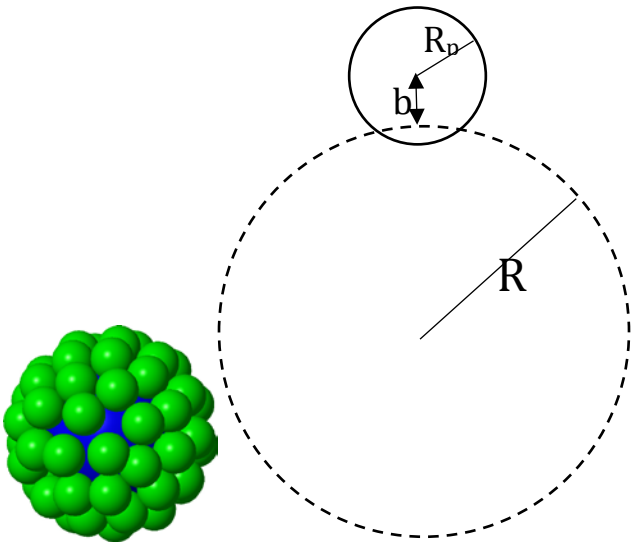

Cartoon for the RaspBerry model.